Proceedings 10th NUMGE 2023
10th European Conference on Numerical Methods in Geotechnical Engineering
Zdravkovic L, Kontoe S, Taborda DMG, Tsiampousi A (eds)

https://doi.org/10.53243/NUMGE2023-198

Periodic random fields to perform site response and liquefaction susceptibility analysis

J.L. González Acosta, D. Varkey, A.P. van den Eijnden, M.A. Hicks

Geo-Engineering Section, Faculty of Civil Engineering and Geosciences,
Delft University of Technology, The Netherlands

ABSTRACT: Free-field site response analysis is a standard technique used to predict soil deposit dynamic response and liquefaction susceptibility. Such analyses are typically carried out by implementing periodic boundaries to guarantee the same speed of the dynamic waves travelling across them. However, when using random fields to consider the impact of soil spatial variability there is the possibility of an inconsistency with periodic boundaries. This is due to the generation of non-identical properties at the lateral boundaries on using traditional random fields. To overcome this inconsistency, this paper proposes periodic random fields to model spatial variability by matching the periodicity at the boundaries. To investigate the significance of using the proposed approach, a heterogeneous soil deposit subjected to earthquake loading is analysed using the random finite element method. The results show that, for certain values of the horizontal scale of fluctuation, ensuring consistency at the lateral boundaries could result in less conservative predictions of the extent of the liquefied areas.

Keywords: Periodic Random Fields; Site Response Analysis; Liquefaction; Tied Degrees

1 INTRODUCTION

A free-field site response analysis (SRA) is a procedure in which the equations of movement are solved for a one-dimensional (1D) column of soil subjected to a base acceleration, typically triggered by earthquake loads. The solution of these equations can be estimated analytically or via finite element (FE) procedures. FE procedures are regularly preferred since they permit the incorporation of diverse and advanced constitutive descriptions and boundary conditions. One important aspect of conducting SRA via FE procedures is the use of special boundaries to simulate the infinity of the domain, hence ensuring an appropriate travelling of the seismic waves from the base of the domain to the ground surface. The two most reliable boundaries in this regard are tied-degrees (TD) and free-field (FF) boundaries. While TD depicts the infinity connecting both sides of the (finite) domain through the global stiffness matrix, FF applies lateral external loads equivalent to those produced by the seismic waves travelling through an isolated and homogeneous 1D column.

It has been observed that TD performs better than FF (Bai and Dong, 2019) since the global connection of both sides of the domain, besides guaranteeing an equal nodal displacement, also takes into account the evolution and changes occurring within the soil such as material degradation or incremental pore water pressures. Unfortunately, despite TDs accuracy, its use is restricted by the fact that both sides of the domain should be identical in terms of geometry and material properties. While geometric differences between both sides of the domain impede the use of TDs, material property variability does not fully restrict its use. The number of studies demonstrating the effectiveness of TD combined with soil spatial variability is extensive (e.g. Popescu et al., 1997; Montgomery and Boulanger, 2016). However, the accuracy of TDs can diminish if the variability of the soil properties increases (González Acosta et al., 2022b). This loss of accuracy results from the inconsistency between the lateral boundaries which, due to the large differences between material properties, behave differently. To overcome this inconsistency, periodicity of the random fields has been introduced in this paper to fulfil the principles of TDs by ensuring identical properties at the lateral boundaries.

In the following sections, the strategies adopted for modelling earthquakes and spatial variability are briefly described. This is followed by the SRA of heterogeneous soil deposit subjected to earthquake loading using the random finite element method (RFEM).

2 METHODOLOGY

A brief description of the FE strategy adopted in this paper for modelling earthquake induced liquefaction and spatial variation of void ratio is given below.

2.1 FE earthquake modelling

In this study, to investigate the undrained cyclic behaviour of the soil, three features are considered: (i) a *u-p* numerical framework; (ii) the hypoplastic constitutive model with intergranular strain for cyclic behaviour (Niemunis and Herle, 1997; Gudehus et al., 2008); and (iii) TD based on the nodal degrees of freedom duplicity. The equation describing the *u-p* FE formulation is

$$\begin{bmatrix} \mathbf{M} & 0 \\ 0 & 0 \end{bmatrix} \begin{Bmatrix} \mathbf{a} \\ \ddot{\mathbf{p}} \end{Bmatrix} + \begin{bmatrix} 0 & 0 \\ \mathbf{Q}^{\mathrm{T}} & \mathbf{S} \end{bmatrix} \begin{Bmatrix} \mathbf{v} \\ \dot{\mathbf{p}} \end{Bmatrix} + \begin{bmatrix} \mathbf{K} & -\mathbf{Q} \\ \mathbf{0} & \mathbf{H} \end{bmatrix} \begin{Bmatrix} \mathbf{u} \\ \mathbf{p} \end{Bmatrix} = \begin{Bmatrix} \mathbf{f} \\ \mathbf{0} \end{Bmatrix} \quad (1)$$

where **M** and **Q** are the mass and hydro-mechanical coupling matrices, respectively, **S** and **H** are the compressibility and permeability matrices of the pore fluid, respectively, **K** is the stiffness matrix of the soil skeleton, **a**, **v** and **u** are the vectors of nodal acceleration, velocity and displacement, respectively, **p** is the vector of water pore pressure where · indicates differentiation, and **f** is the vector of internal and external forces. A detailed explanation of the *u-p* formulation, including time discretization, can be found in Zienkiewicz et al. (1999). Also, note that in this paper upper case and lower case bold letters indicate matrices and vectors, respectively. With respect to the implementation of TD, the procedure explained in Cook et al. (1989) is used. In this case, the left and right side nodes of the domain can be tied by duplicating the degree of freedom (dof) of the corresponding nodes as seen in Figure 1, where a row of square elements, with one dof per node, has been tied at both sides. Following this approach, the domain will be tied automatically during the construction of the global stiffness matrix.

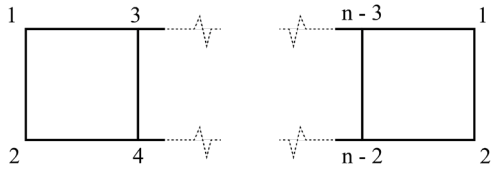

Figure 1. Implementation of TD with a single dof shared between the nodes on the left and right domain boundaries

2.2 Modelling spatial variability

In this paper, spatial variability in void ratio has been considered during the SRA of a soil deposit. The spatial variability can be quantified using a parameter called the scale of fluctuation (θ), which approximately defines the distance over which property values are significantly correlated and which can be mathematically represented using random fields (Vanmarcke, 1983). Random fields of void ratio ($\boldsymbol{e}$) for the domain have been generated using

$$\mathbf{e} = \mu_e + \mathbf{z} \times \sigma_e, \text{ where } \mathbf{z} = \mathbf{A} \times \boldsymbol{\xi} \quad (2)$$

where μ_e and σ_e are the mean and standard deviation, respectively, of a normal distribution of void ratio, **z** is a vector of standard normal random field values, $\boldsymbol{\xi}$ is a vector of standard normal random numbers and **A** is the decomposed covariance matrix. The covariance matrix is traditionally generated using

$$\beta(\tau_{\mathrm{h}}, \tau_{\mathrm{v}}) = \sigma_e^2 \times \exp\left(-\sqrt{\left(\frac{2\tau_{\mathrm{h}}}{\theta_{\mathrm{h}}}\right)^2 + \left(\frac{2\tau_{\mathrm{v}}}{\theta_{\mathrm{v}}}\right)^2} \right) \quad (3)$$

where τ_{h} and τ_{v} are the lag distances, and θ_{h} and θ_{v} are the scales of fluctuation, in the horizontal and vertical directions, respectively.

An ensemble of random fields is generated to represent uncertainty in the spatial distribution, and the random fields are coupled with finite elements using RFEM to perform the SRA of heterogeneous soil deposits subject to earthquake loading. However, this coupling results in an inconsistency as the fundamental assumption of TD, requiring the lateral vertical boundaries to be identical, is no longer valid. To overcome this inconsistency, periodic random fields are instead proposed herein to model the spatial variability. Here, the periodicity of the random fields matches the width (W) of the domain to ensure consistency with TD fundamentals of the FE model. The periodic random fields have been generated using the following covariance function:

$$\beta(\tau^*_{\mathrm{h}}, \tau_{\mathrm{v}}) = \sigma_e^2 \times \exp\left(-\sqrt{\left(\frac{2\tau^*\mathrm{h}}{\theta_{\mathrm{h}}}\right)^2 + \left(\frac{2\tau_{\mathrm{v}}}{\theta_{\mathrm{v}}}\right)^2} \right) \quad (4)$$

where

$$\tau^*_{\mathrm{h}} = \min(\tau_{\mathrm{h}}, W - \tau_{\mathrm{h}}) \quad (5)$$

Figure 2 shows typical realisations of (a) traditional (non-periodic) random fields (RF) and (b) periodic random fields (PRF) of void ratio random fields generated for a domain of size 20 m × 10 m by using θ_{h} = 5 m and θ_{v} = 1 m which are within the range of values of θ typically observed in practice. Also shown in the figure are the values of void ratio (e) and shear wave velocity (V_s) generated along the two lateral boundaries (i.e. A-A and B-B). As observed in Figure 2(a), shear wave velocities differ at the ends of the domain when periodicity is not considered. This difference conflicts with the fundamentals of using TD. On the other hand, when periodicity is considered, both sides of the domain describe similar V_s distributions, ensuring TD fundamentals and therefore guaranteeing an adequate seismic wave propagation.

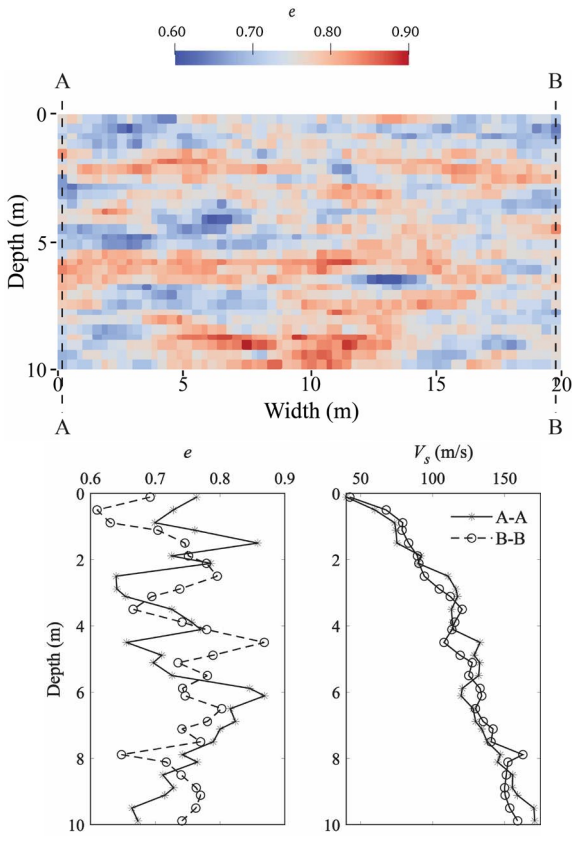

(a) Random Field (RF)

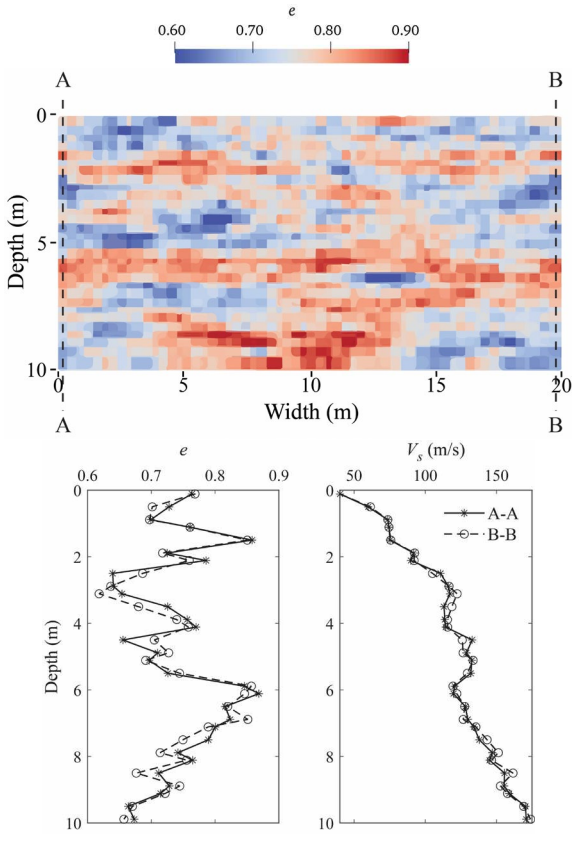

(b) Periodic Random Field (PRF)

Figure 2. Typical realisations of random fields generated within the domain using θ_h = 5 m and θ_v = 1 m

Figure 3 shows the covariances back-calculated from the realisations in Figure 2. As shown in the figure, the values at the lateral ends of the domain that were generated using the periodic random fields are correlated to each other while preserving the theoretical correlation structure.

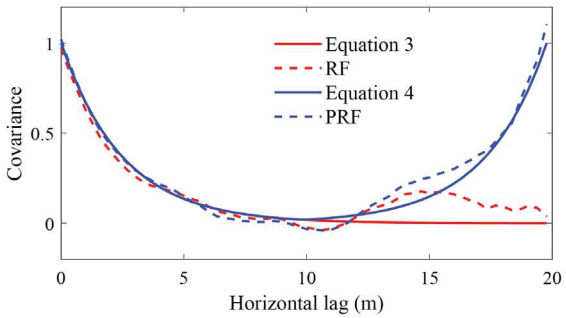

Figure 3. Covariance of the void ratios back-calculated from the realisation in Figure 2

3 NUMERICAL EXPERIMENT

In this section, the influence of spatial variability of void ratio on SRA using random fields is demonstrated for a domain of size 20 m × 10 m. The random fields of void ratio are generated using a mean of 0.75, a vertical scale of fluctuation of 1 m and different values of the standard deviation and the horizontal scale of fluctuation. For each case, two sets of 500 realisations of random fields are generated (one using periodic boundary conditions and one using non-periodic boundary conditions). Earthquakes are simulated using the accelerations recorded during the 1999 Chi-Chi earthquake in Taiwan. At the end of the earthquake, the total area that has undergone liquefaction is computed as:

$$A_L = \mathrm{I}\left(\frac{u}{\sigma'_{v0}} \geq 0.95\right) \times \frac{100}{n} \tag{6}$$

where A_L is the percentage liquefied area, I(.) is the indicator function which is equal to 1 if the condition within the brackets is true and 0 otherwise, u and σ'_{v0} are the excess pore water pressure and the initial vertical effective stress, respectively, at an integration point, and n is the total number of integration points in the domain. In this study, square elements of size 1 m × 1 m, with nine nodes and nine integration points have been used.

Table 1. Hochstetten sand parameters

Parameter	Value	Units
φ_c	33	°
p_t	1.0E^{-5}	kPa
h_s	1.5E^{6}	kPa
n	0.28	-
e_{d0}	0.55	-
e_{c0}	0.95	-
e_{i0}	1.05	-
α	0.25	-
β	1.5	-
m_R	5.0	-
m_T	2.0	-
R	1.0E^{-4}	-
β_r	0.5	-
χ	6.0	-

Regarding material properties, Hochstetten sand (which has been validated to perform cyclic simulations) has been selected to perform the SRA. In this study, a specific gravity (G_s) of 2.65 has been considered together with the values in Table 1 (Mašín, 2019). The soil density can be computed using the values of G_s and e. Finally, the domain is subjected to the base acceleration shown in Figure 4. Since most of the acceleration record can be considered inconsequential, a time window between 10 and 20 s was considered.

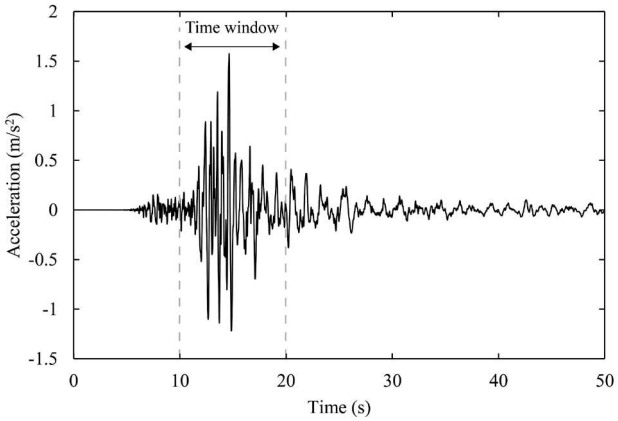

Figure 4. 1999 Chi-Chi earthquake (station CHY074, component 0, PGA = 154.51 cm/s^2)

3.1 Results

Figure 5 shows the probability density function of A_L computed from the 500 realisations generated using a standard deviation of 0.06 and different values of θ_h. Also shown in the figure is the deterministic solution based on the mean void ratio obtained from the SRA of a one-dimensional homogeneous column. The results show that the values of A_L obtained by accounting for spatial variability using 2D RFEM are significantly larger than the deterministic solution. This difference is due to the limitation of 1D columns in preventing the spread of liquefaction in the vertical direction, hence giving unreliable results (see González Acosta et al. (2022a) for more details).

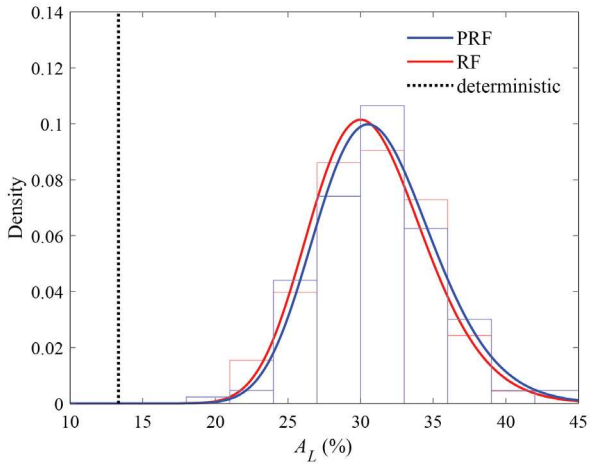

(a) θ_h = 1 m

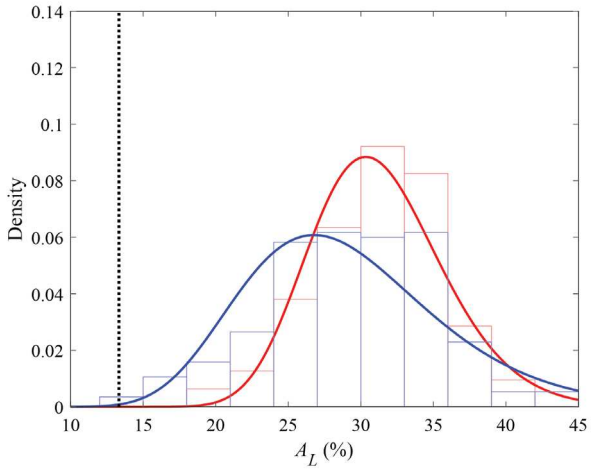

(b) θ_h = 5 m

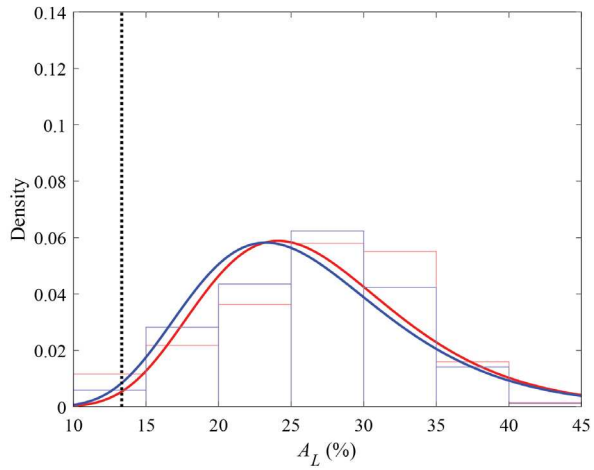

(c) θ_h = 10 m

Figure 5. Distributions of liquefied area (A_L) obtained using periodic (PRF) and non-periodic (RF) random fields generated using various values of θ_h

It can be observed that the mean values of A_L obtained in the 2D simulations using RFEM approach the deterministic solution as θ_h increases, although the differences remain very large. It can also be observed that the difference between the results using PRF and

RF is not significant when θ_h = 1 m and θ_h = 10 m. When θ_h is very small with respect to the width (W) of the domain, small pockets of loose and dense sand are generated throughout the domain in each realisation without forming a clear pattern, reducing the importance of using periodic random fields and giving a large A_L mean value as a consequence of the multiple triggering spots created. Conversely, with large values of θ_h, for example θ_h = 10 m (i.e. $\theta_h >= W/2$), various semi-continuous zones of loose and dense sands are generated. Liquefaction is triggered rapidly in the looser zones and this hinders further spreading in the domain, thereby resulting in a smaller mean A_L value.

However, on using θ_h = 5 m (=W/4), i.e. an intermediate value of θ_h with respect to W, the mean A_L value obtained using PRF is smaller than that using RF. This is because, by being consistent with TD using PRF, extended zones of loose sand are created which provoke a rapid liquefaction triggering along the entire width of the domain, thus preventing the seismic waves from travelling vertically and causing further spreading of liquefaction. This results in smaller values of A_L than the over conservative solutions obtained using RF.

For example, for the realisations of void ratio using RF and PRF shown in Figure 2, generated using θ_h = 5 m, Figure 6 illustrates the evolution of liquefaction with time. Due to the presence of a wider preferential path of loose sand at depth ≈ 6 m using PRF (see Figure 2b), liquefaction already occurs at t = 4.5 s (see Figure 6a) over almost the entire width of the domain, covering an area of 8.7% compared to only 6.3% using RF. However, with the passage of time (see Figure 6(b–c)), liquefaction spreads over a smaller area using PRF compared to that using RF. This is due to the rapid triggering of liquefaction using PRF, reducing the upward spread of seismic waves and thereby reducing the further spread of liquefaction in the domain.

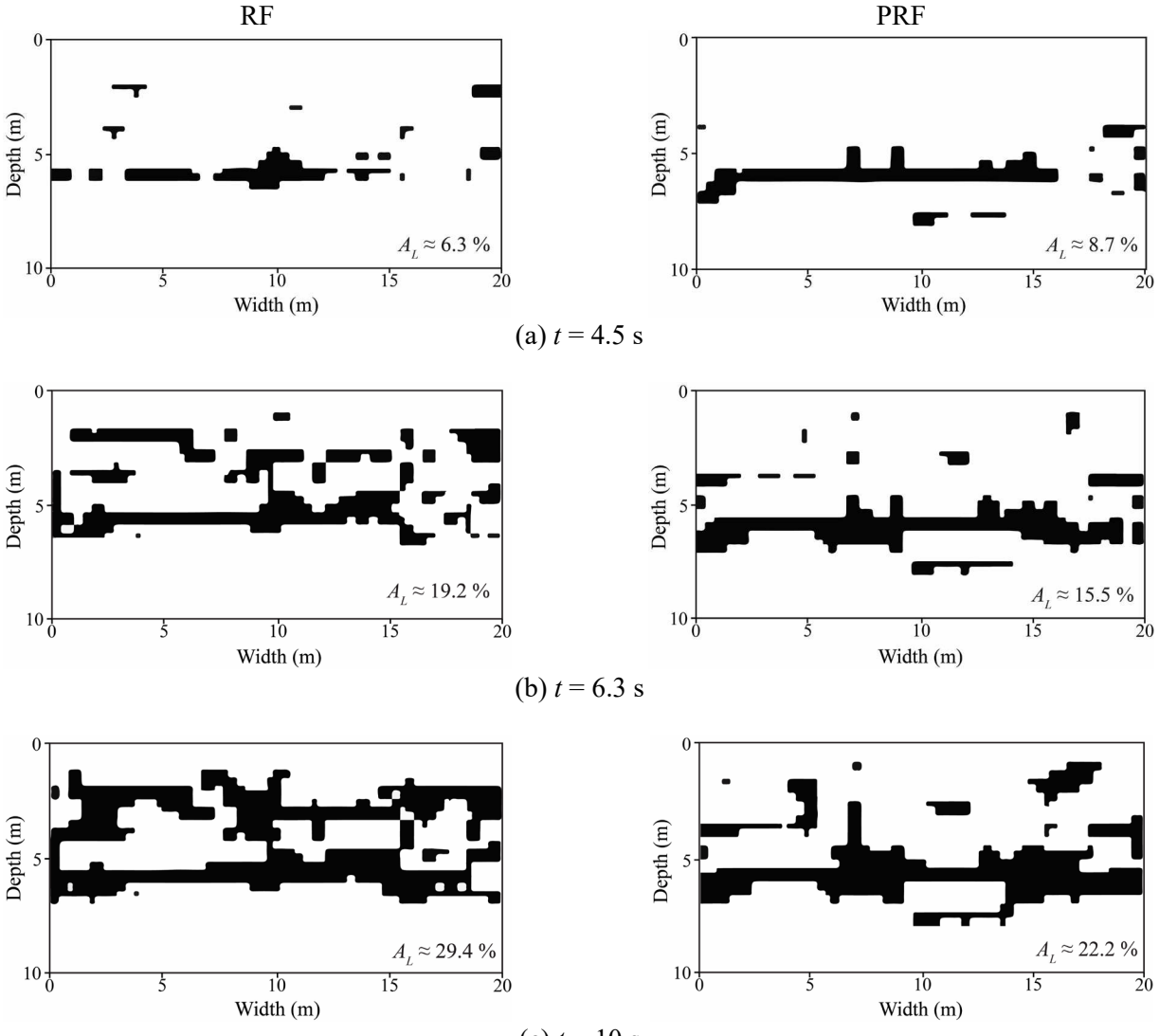

Figure 6. Evolution of liquefaction with time for the realisations in Figure 2. The left and right columns show the liquefied areas (indicated by black zones) obtained using RF and PRF, respectively.

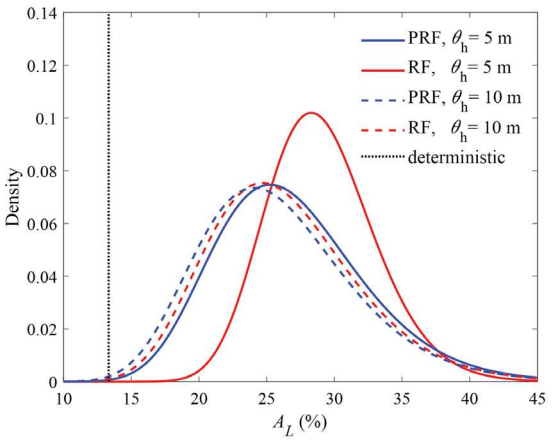

(a) $\sigma_e = 0.04$

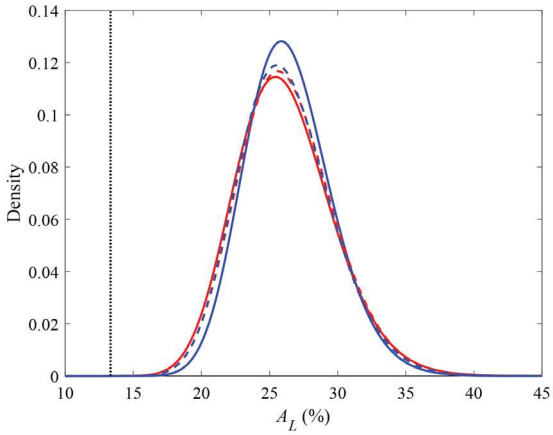

(b) $\sigma_e = 0.02$

Figure 7. Distributions of A_L obtained using PRF and RF generated using various values of θ_h and standard deviations of the void ratio

Finally, the results in Figures 5 and 6 are based on using a standard deviation (σ_e) of 0.06 for void ratio, which is a much larger value than that reported in literature. The sensitivity of the results to spatial variability becomes much less apparent when using a much smaller value of the standard deviation, as is shown in Figure 7. The range of values of θ_h for which using PRF and RF results in significantly different responses needs further investigation.

4 Conclusions

A methodology for modelling earthquake induced liquefaction while accounting for spatial variability has been presented in this paper. The spatial variability in void ratio is modelled using random fields. Periodicity has been introduced in the random fields that matches the size of the domain to ensure the consistency required to implement tied-degrees of freedom. The results obtained by considering spatial variability show a significant difference from those obtained in a deterministic analysis based on the mean properties. Furthermore, it has been demonstrated that considering periodicity in the random fields can result in less conservative predictions.

5 Acknowledgements

This work is part of the research programme DeepNL/SOFTTOP with project number DEEP.NL.2018.006 which is financed by the Netherlands Organisation for Scientific Research (NWO), and was carried out on the Dutch National e-infrastructure with the support of SURF Foundation.

6 References

Bai, J.F., Dong, S.X. 2019. Selection of lateral artificial boundary distance and its influence on the site seismic responses analysis. *Proc, IACGE* (Eds: Hu, J., Zhang, W., Yu, X., Liu, H.), 70–84. American Society of Civil Engineers, Reston VA. 10.1061/9780784482049.008

Cook, R.D., Malkus, D.S., Plesha, M.E. 1989. *Concepts and applications of finite element analysis*, John Wiley & Sons, New York.

González Acosta, J.L., van den Eijnden, A.P., Hicks, M.A. 2022a. Comparison of 1D and 2D liquefaction assessment methods considering soil spatial variability, *Proc, 8th ISGSR* (Eds: Huang, J., Griffiths, D.V., Jiang, S.H., Giacomini, A., Kelly, R.), 773–778. Research Publishing, Singapore.10.3850/978-981-18-5182-7_14-001-cd

González Acosta, J.L., van den Eijnden, A.P., Hicks, M.A. 2022b. Liquefaction assessment and soil spatial variation. *Proc, 16th IACMAG* (Eds: Barla, M., Di Donna, A., Sterpi, D., Insana, A.), 283–290. Springer, Cham. 10.1007/978-3-031-12851-6_34

Gudehus, G., Amorosi, A., Gens, A., Herle, I., Kolymbas, D., Mašín, D., Wood, D.M., Niemunis, A., Nova, R., Pastor, M., Tamagnini, A., Viggiani, G. 2008. The soilmodels.info project. *Int J Numer Anal Methods Geomech*, 32, 1571–1572. 10.1002/nag.675

Mašín, D. 2019. *Modelling of soil behaviour with hypoplasticity - another approach to soil constitutive modelling,* Springer Cham, Switzerland.

Montgomery, J., Boulanger, R.W. 2016. Effects of spatial variability on liquefaction-induced settlement and lateral spreading. *J Geotech Geoenvironmental Eng - ASCE*, 143: 04016086. 10.1061/(ASCE)GT.1943-5606.0001584

Niemunis, A., Herle, I. 1997. Hypoplastic model for cohesionless soils with elastic strain range. *Mech Cohesive-Frictional Mater*, 2, 279–299. 10.1002/(SICI)1099-1484(199710)2:4%3C279::AID-CFM29%3E3.0.CO;2-8

Popescu, R., Prevost, J.H., Deodatis, G. 1997. Effects of spatial variability on soil liquefaction: some design recommendations. *Géotechnique*, 47: 1019–1036. 10.1680/geot.1997.47.5.1019

Vanmarcke, E.H. 1983. *Random fields: analysis and synthesis*. The MIT Press, Cambridge, Massachusetts.

Zienkiewicz, O.C., Chan, A.H.C., Pastor, M., Schrefler, B. A., Shiomi, T. 1999. *Computational geomechanics with special reference to earthquake engineering*, John Wiley & Sons, New York.